

Effect of Alkyl-Chain-Length on the Electrochemical Behavior and Diffusion Coefficient of Imidazole- and Pyridine-Based Surfactants in Aqueous Solutions

A. R. Lara-Hernández¹, N. V. Gallardo-Rivas^{1,*}, U. Páramo-García¹, R. Mayen-Mondragon², S. B. Brachetti-Sibaja¹

¹ Tecnológico Nacional de México/I. T. Cd. Madero, Centro de Investigación en Petroquímica, Prol. Bahía de Aldhair y Av. de las Bahías, Parque de la Pequeña y Mediana Industria, 89600, Altamira, Tamaulipas, MÉXICO

² Polo Universitario de Tecnología Avanzada, Facultad de Química, Universidad Nacional Autónoma de México, Vía de la Innovación 410, Autopista MTY-Aeropuerto Km. 10, Parque PIIT, 66629, Apodaca, Nuevo León, MÉXICO.

*E-mail: nohra.gr@cdmadero.tecnm.mx

Received: 2 May 2021 / Accepted: 12 June 2021 / Published: 10 September 2021

In the present work, imidazole and pyridine-based surfactants were successfully synthesized at our laboratory by a two-staged reaction mechanism of cation formation followed by anion exchange. Their molecular structure was confirmed by Fourier Transform Infrared Spectroscopy with Attenuated Total Reflectance and Nuclear Magnetic Resonance Spectroscopy. The diffusion coefficient of the surfactants was determined by linear sweep voltammetry at the rotating-disk-electrode, using the Koutecky-Levich equation. The results showed an alkyl-chain-length increase leads to a diffusion coefficient decrease (C6 > C12 > C18). This is due to the increase in hydrophobicity and molecular weight of the molecule, which hinders micelle transport towards the working electrode. The similar electrochemical behavior of the imidazole- and pyridine-based compounds can be associated with their chemical structure and electron density in the aromatic ring.

Keywords: Surfactant, imidazole, pyridine, diffusion coefficients, rotating disk electrode.

1. INTRODUCTION

Scientific research on surfactants has increased in recent years due to their wide application in the extraction and transportation of crude oil [1], modification of surface phenomena of immiscible systems [2] and recovery of hydrocarbon-contaminated soils [3].

Surfactants are organic compounds with an amphiphilic structure, i.e. their molecules contain polar (hydrophilic) and nonpolar (hydrophobic) groups. Such characteristic promotes, within low

miscibility systems, the interaction of different phases with each other [1]. Thus, they can form micelles with high chemical and thermodynamic stability, and they can be used as foaming, emulsifying, and dispersing agents [4].

Surfactants are composed of organic cations such as imidazole, pyridine, and pyrazole [5]. The anionic counterpart can have an organic/inorganic nature such as bromine and chlorine, or large compounds such as tetrafluoroborate, hexafluoroborate, and p-toluenesulfonate [6]. The selection of each member depends on the desired physicochemical properties (density, viscosity, surface tension, hydrophobic-hydrophilic interaction) of the surfactant [7]. One of the most important characteristics of surfactants is their capability to form micelles, which depends on their concentration in aqueous solution [3].

According to the literature, electrochemical methods have been successfully applied to study micellization processes and related parameters such as diffusion coefficient, hydrodynamic radius, micelle aggregation number and critical micelle concentration [8, 9]. Cyclic voltammetry, for example, can follow the micellization of surfactant molecules based on the oxidation-reduction processes which they sustain, while promoting mass transport towards the working electrode [10]. On the other side, the study of micellar hydrodynamic movement can be performed with the Rotating Disk Electrode (RDE), which may help study independently the diffusion and convection phenomena present during solution agitation (50 to 10,000 rpm) [11]. For example, the diffusion coefficient of brominated surfactants can be determined by analyzing the measured peak current as a function of electrode rotation rate [12]. The electrochemical behavior of the cationic-surfactant cetyl-trimethylammonium-bromide (CTAB) on a glassy carbon electrode has as well been investigated by cyclic voltammetry at the rotating disk electrode [13, 14]. For such a system, the thickness of the diffusion layer was determined by using Levich's equation [13].

The present work studies the electrochemical behavior of imidazole- and pyridine-based surfactants by cyclic voltammetry, and linear sweep voltammetry at the rotating disk electrode. The respective diffusion coefficients were determined and associated to the effect of hydrocarbon chain length (C_6 , C_{12} , C_{18}) on the micellization processes.

2. EXPERIMENTAL

2.1. Materials

1-Methylimidazole (Sigma Aldrich, 95%) and 2-methylpyridine (Sigma Aldrich, 98%) were selected as cations due to their high chemical and thermal stability, as well as amphoteric nature [15]. Sodium p-toluenesulfonate (Sigma Aldrich, 95%) was used as anion generator and thus it is responsible for the chemical properties and reactivity of the molecule [16]. 1-Bromohexane (Sigma Aldrich, 98%), 1-bromododecane (Sigma Aldrich, 97%) and 1-bromooctadecane (Sigma Aldrich, 97%) were used as alkyl-chain-length modifiers (C_6 , C_{12} , C_{18}).

2.2. Synthesis of surfactants

Figure 1 shows the two-staged reaction-mechanism of surfactant synthesis: cation formation (1a) and anion exchange (1b) [17-19].

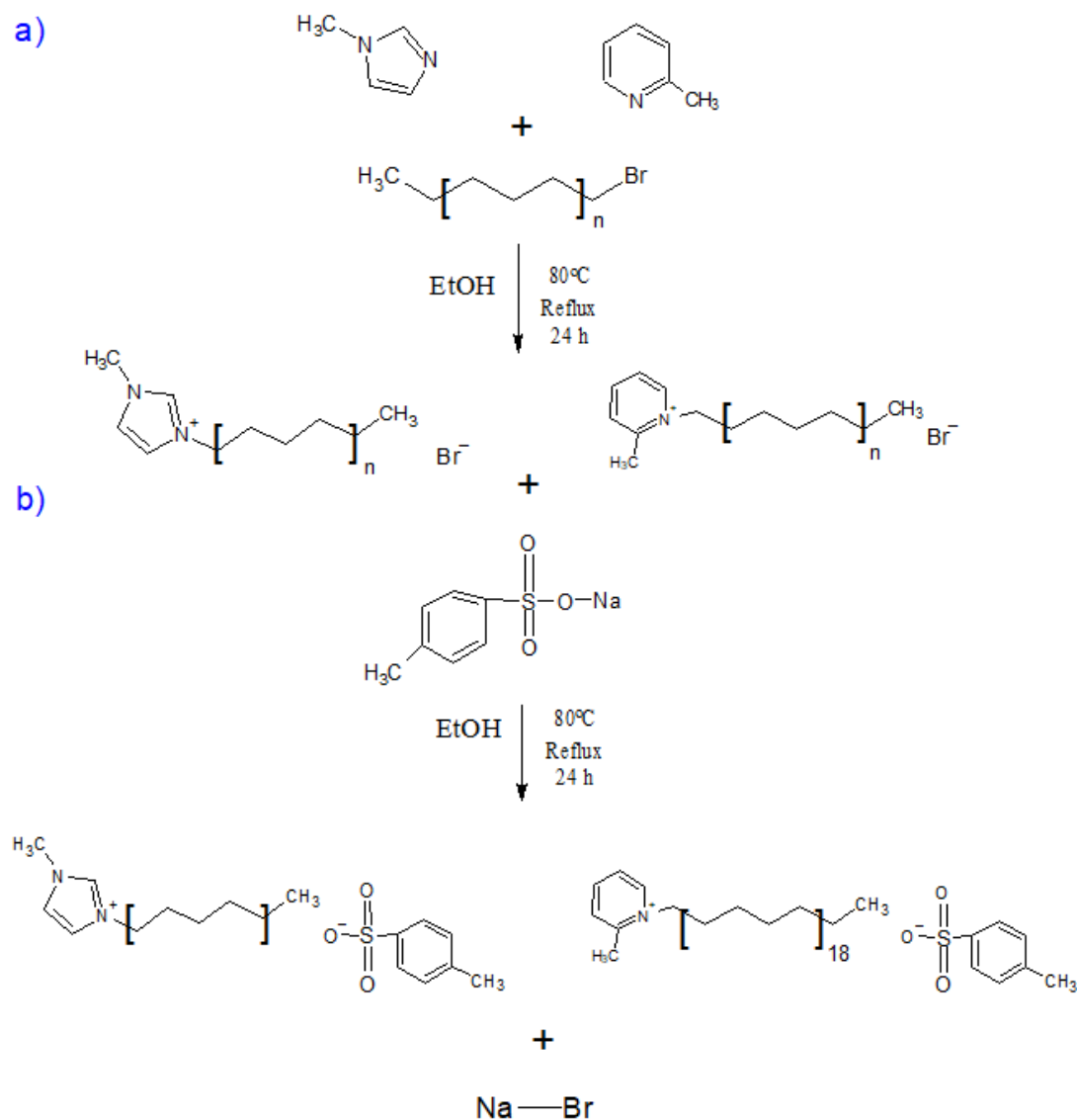
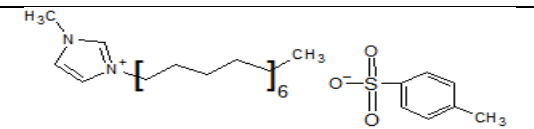
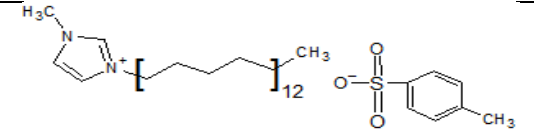
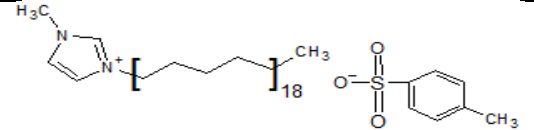
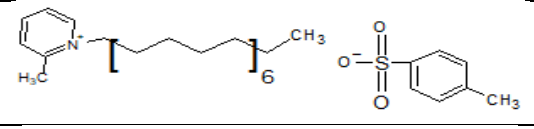
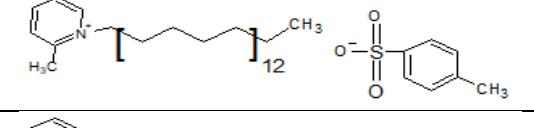
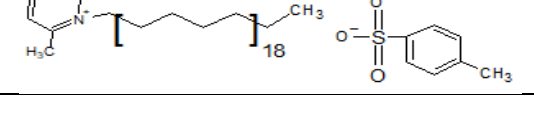


Figure 1. Two-staged reaction-mechanism of imidazole- and pyridine-based surfactants synthesis: a) cation formation and b) anion exchange.

Imidazole/pyridine reacts within the first stage with the alkyl bromides (1:1 Molar ratio) in the presence of ethanol at 80 °C during 24 h. The bromide is afterwards exchanged for the p-toluenesulfonate group by means of a double substitution reaction in the presence of ethanol at 80 °C during 24 h. After completing the reaction, the solvent was removed by vacuum evaporation using a rotary evaporator at 85 °C during 4 h. Sodium bromide was eliminated by subsequent filtration cycles. The chemical structure of the synthesized surfactants is presented in Table 1. The structure was confirmed by Fourier Transform Infrared Spectroscopy with Attenuated Total Reflectance (FTIR-ATR) and Nuclear Magnetic

Resonance (NMR) Spectroscopy. For the former, a Perkin Elmer Spectrum One spectrometer was used applying 12 scans from 4000 to 400 cm^{-1} . For the latter, a Bruker Ascend 400 MHz spectrometer was used along with deuterated water as solvent [20, 21].

Table 1. Molecular structure of the imidazole- and pyridine-based surfactants synthesized by the two-staged reaction-mechanism shown in Figure 1.

Code	TA's	Chemical structure
C6IMI	1-methyl-3-hexylimidazolium p-toluenesulfonate.	
C12IMI	1-methyl-3-dodecylimidazolium p-toluenesulfonate.	
C18IMI	1-methyl-3-octadecylimidazolium p-toluenesulfonate.	
C6PYR	2-methyl-5-hexylpyridinium p-toluenesulfonate	
C12PYR	2-methyl-5-dodecylpyridinium p-toluenesulfonate	
C18PYR	2-methyl-5-octadecylpyridinium p-toluenesulfonate	

2.3. Cyclic voltammetry

Electrochemical measurements were performed using a BASi 100 B/W electrochemical analyzer and a three-electrode system consisting of a glassy carbon electrode (MF-2012, 3 mm diameter, BASi) as working electrode, a saturated Ag/AgCl reference electrode (MF-2052, BASi) and a platinum wire as counter electrode (MW-1032, BASi) [22]. The working electrode was mechanically polished with alumina of different sizes (MF-2051, 15 μm ; MF-2059, 3 μm ; MF-2054, 1 μm , BASi) prior to each run. Voltammograms were recorded for each surfactant solution (10 g L^{-1}) within a potential window of -1.0 to 1.0 V, starting from 0 V towards the oxidation region, and at a scan rate of 10 mV s^{-1} . All measurements were conducted at room temperature [23-25].

2.4. Rotating Disk Electrode

A glassy carbon rotating disk electrode (RDE-2, 3 mm, BASi) was used as working electrode, together with a saturated Ag/AgCl reference electrode (MF-2052, BASi), and a Pt wire as counter electrode (MW-1032, BASi). Voltammograms were recorded for each surfactant solution (10 g L⁻¹) within a potential window of 0 to 1.0 V at 10 mV s⁻¹, applying rotation rates from 100 to 1000 rpm at 100 rpm steps. All measurements were conducted at room temperature. The reciprocal-current-density J_a^{-1} at different selected potentials was used to determine the diffusion coefficient [12, 26, 27] according to the Koutecky-Levich (1) equation:

$$\frac{1}{J_a} = \frac{1}{0.620nFD_0^{2/3}v^{-1/6}C_0} \omega^{-1/2} \quad (1)$$

Where n is the number of transferred electrons, F is the Faraday constant, ω is the rotation rate (rpm), v is the kinematic viscosity (cm² s⁻¹), C_0 is the analyte concentration (mol cm⁻³) and D_0 is the analyte diffusion coefficient (cm² s⁻¹). D_0 was calculated from the slope m of the J_a^{-1} vs $\omega^{-1/2}$ plot, applying Equation 2 [13, 28]:

$$D_0 = \left(\frac{1}{0.620 nmFv^{1/6}C_0} \right)^{3/2} \quad (2)$$

3. RESULTS AND DISCUSSION

3.1. Characterization methods

3.1.1. FTIR analysis

The FTIR spectra of the imidazole- and pyridine-based synthesized surfactants are shown in Figure 3a and Figure 3b, respectively. The 3407 and 3410 cm⁻¹ transmittance bands are attributed to the N-H stretching mode of imidazole and pyridine, respectively [20, 29]. The bands at 2927, 2860, 2930 and 2875 cm⁻¹ are associated to the symmetric and asymmetric CH₂ and CH₃ stretching modes. Bands between 1659 and 1487 cm⁻¹ are related to the aromatic C=C stretching modes, confirming thus the presence of the benzene ring. The C=N stretching modes at 1560 and 1587 cm⁻¹, and C-N bending mode at 1123 cm⁻¹ are associated with the nitrogen heterocycle within the cationic member. S=O stretching modes at 1167, 1027, 1183 and 1042 cm⁻¹ are assigned to the SO₃⁻ group. The C-H bending modes at 830 and 796 cm⁻¹, indicating a p- (para) orientation of the benzene ring, are characteristic of the synthesized compounds [30-31].

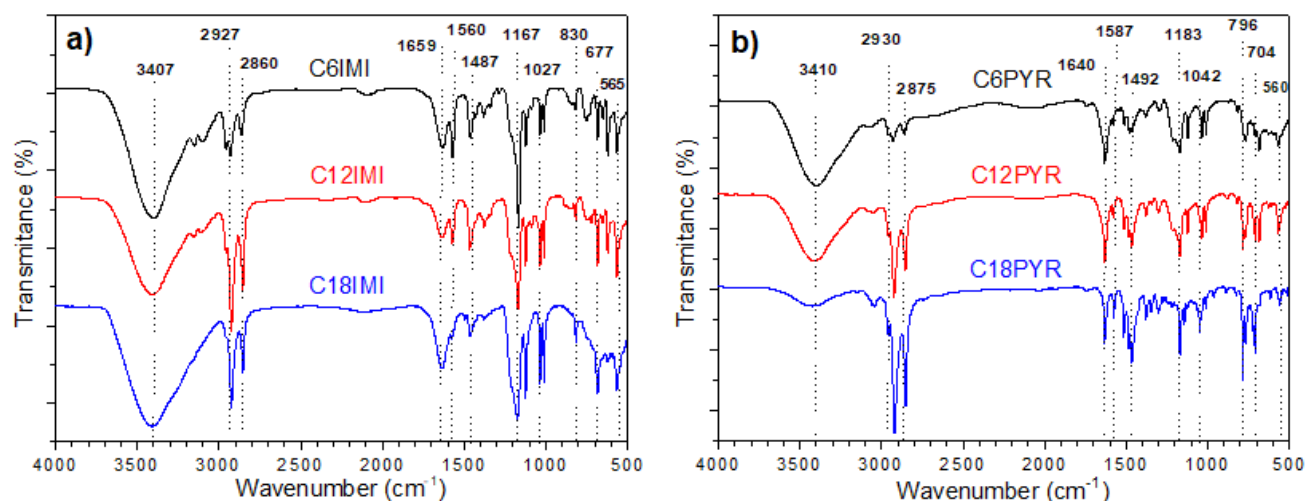


Figure 3. FTIR spectra of synthesized surfactants: a) imidazole-based- and b) pyridine-based-cation (see Table 1).

3.1.2. Nuclear Magnetic Resonance Spectroscopy.

The NMR spectrum of the C6IMI is shown in Figure 4a [21, 33-35]: ^1H -RMN (400 MHz, D_2O) δ (ppm): 0.86 (t, 3H), 1.28-1.40 (d, 2H), 1.91-1.97 (m, 4H), 2.36 (t, 3H), 3.10 (s, 1H), 3.40 (t, 3H), 4.62 (t, 2H), 4.86 (d, 1H), 4.96 (d, 1H), 7.47 (d, 2H), 7.95 (d, 2H). ^{13}C -RMN (100 MHz, D_2O) δ (ppm) is shown in Figure 4b: 14.02, 21.13, 22.94, 27.79, 28.29, 31.65, 46.62, 121.06, 124.29, 126.74, 128.77, 137.50, 138.50, 149.67. The NMR spectra of the surfactants are detailed in the supplementary information appendix.

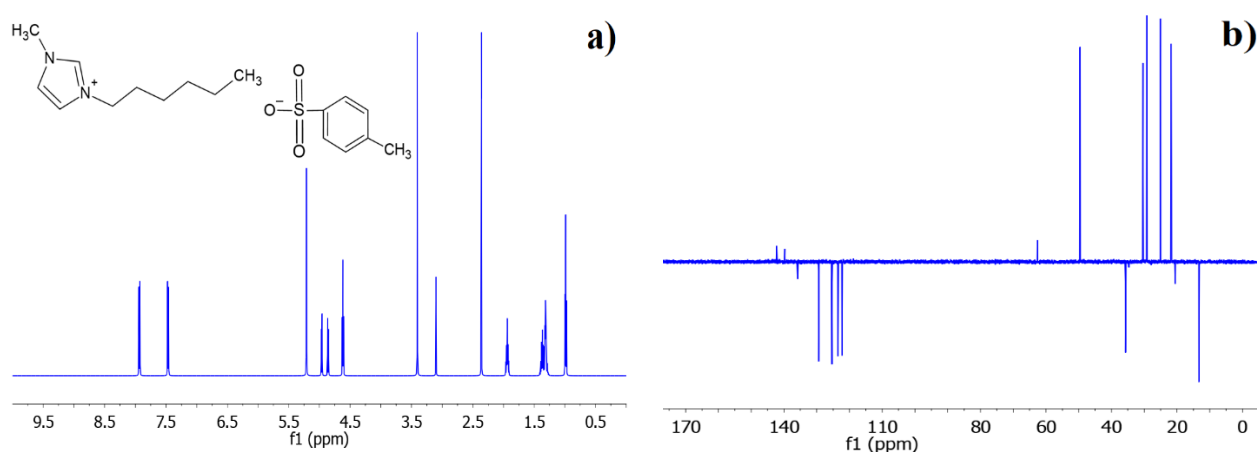


Figure 4. NMR spectrum of the synthesized C6IMI imidazole-based surfactant: a) ^1H -RMN and b) ^{13}C -RMN.

3.2. Cyclic voltammetry

Cyclic voltammograms of the synthesized imidazole-based- and pyridine-based-surfactants are presented in Figures 5a and 5b, respectively. Figure 5a shows an oxidation process starting at around 0.81 V. It is associated with the p-toluensulfonate anionic member, as one of its electrons (O^*) is transferred to the imidazolium cation. The respective process rate is modulated by the hydrocarbon chain length as well as by its associated electron density [23]. The oxidation peak-current-density is achieved at 0.92 V for C6IMI, 0.9 V for C12IMI, and 0.88 V for C18IMI. Comparatively, the reduction peak-current-density is achieved at -0.5 V for C6IMI, -0.45 V for C12IMI and -0.35 V for C18IMI. Reduction peaks of surfactants are significantly shifted to more positive potentials as the hydrocarbon chain length increases [36]. The latter favors the molecule hydrophobicity and, as a consequence, micelle formation and growth [37-39]. At the same time, as the size of micellar aggregates changes, the peak current density decreases [40, 41]. The variation of the molecules solubility in aqueous medium affects their transport towards the working electrode, so the overall diffusion-convection processes are effectively slowed-down [38, 42, 43].

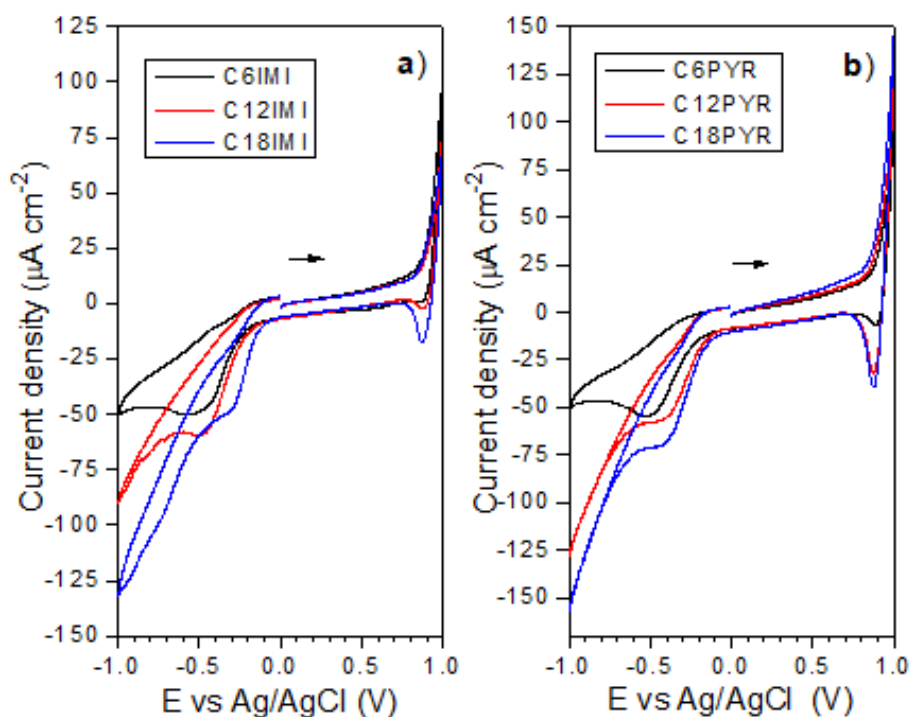


Figure 5. Cyclic voltammograms of (a) imidazole- and (b) pyridine-based synthesized surfactants, 10 g L^{-1} aqueous solutions, scan rate: 10 mV s^{-1} (glassy carbon working electrode, saturated Ag/AgCl reference electrode, platinum wire counter electrode).

The length of the hydrocarbon chain may affect other physicochemical properties in addition to the molecule solubility, such as the electric conductivity [38, 39].

Figure 5b shows the redox processes of the pyridine-based compounds. The oxidation, associated with the p-toluensulfonate group, starts at around 0.8 V vs. Ag/AgCl where one of its electrons (O^*) is transferred to the pyridinium cation [44, 45]. At first, the maximum current density is reached in the anionic phase, followed by the reduction process of the pyridinium cation at 0.91 and -0.51 V for C6PIR, 0.87 and -0.43 V for C12PIR, 0.85 and -0.41 V for C18PIR.

3.3. Rotating disk electrode

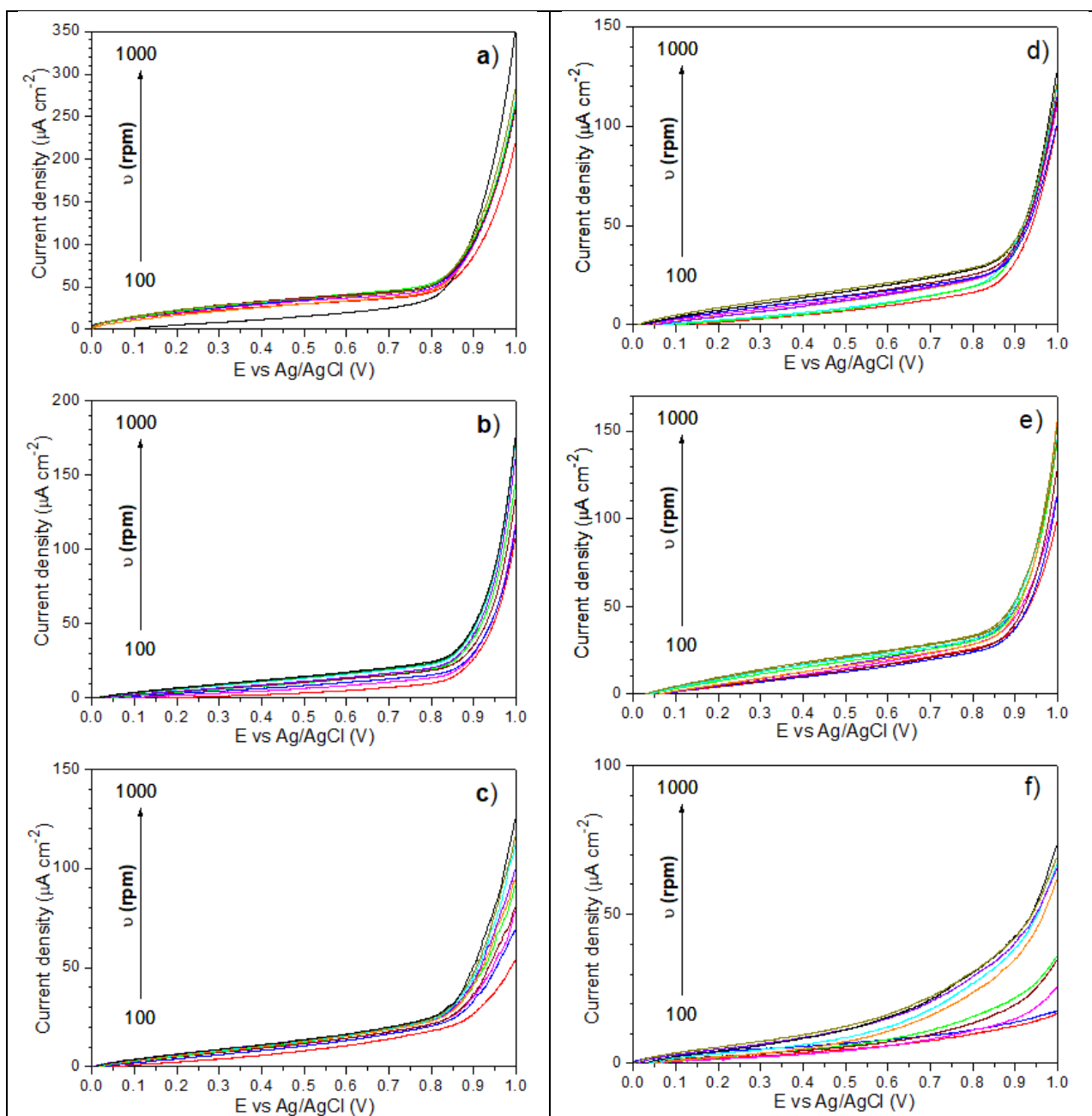


Figure 6. Linear-sweep oxidation voltammograms of imidazole- and pyridine-based synthesized surfactants, 10 g L^{-1} aqueous solutions, scan rate: 10 mV s^{-1} (glassy carbon working electrode, saturated Ag/AgCl reference electrode, platinum wire counter electrode). Electrode rotation-rate interval: 100 to 1000 rpm. a) C6IMI, b) C12IMI, c) C18IMI, d) C6PYR, e) C12PYR, f) C18PYR.

The linear sweep voltammograms of the synthesized imidazole-based- and pyridine-based surfactants at varying electrode rotation-rates are shown in Figure 6. The higher the rotation rate, the higher the observed current density due to the shorter diffusion-layer thickness and thus a faster transport of surfactant species towards the working electrode. The generation of a double layer of micellar aggregation is thus favored [40, 46]. In general, the charge-transfer-control region for these electrochemically irreversible systems can be found between 0.1 and 0.8 V. Within such a region, the oxidation-reduction processes in the aqueous system are mainly controlled by the electron transfer kinetics at the electrode/electrolyte interface. The mixed-control region, where both charge transfer and mass transfer occur at a similar rate, is expected within a smaller voltage range between 0.8 and 1 V; finally, the mass-transfer-control region is expected at potentials higher than 1 V. The similar electrochemical response of the imidazole- and pyridine-based synthesized surfactants is due to the structural and electronic similarity of the imidazole and pyridine molecules. Both behave as nitrogen heterocycles showing electron delocalization within the aromatic ring as well as an electronic absorption effect [44, 47-48].

3.4. Surfactants diffusion coefficient

When the rate of a half-reaction occurring at an electrode surface is limited by a combination of mass transport and slow kinetics, it is often possible to use the rotating disk electrode to elucidate transport parameters (e.g. diffusion coefficient) as well as kinetic parameters (e.g. standard rate constant) from a Koutecky-Levich study [27, 49, 50].

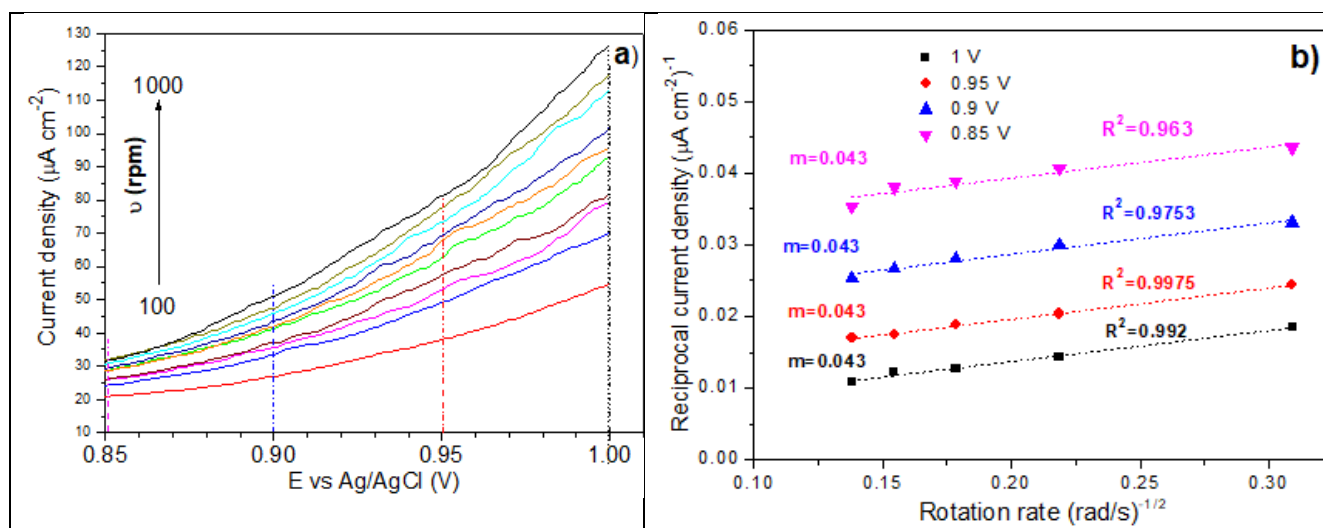


Figure 7. Koutecky-Levich analysis of the C18IMI surfactant. a) Rising section of the voltammogram-anodic-region (Figure 6c) showing the current-density sampling-potentials (0.85, 0.9, 0.95 and 1 V), b) Koutecky-Levich plot of the sampled data from Figure 7a.

Figure 7a shows the rising section of the C18IMI voltammogram-anodic-region at the different electrode-rotation-rates tested. The current density was sampled at four different potentials (0.85, 0.9,

0.95 and 1V) in order to derive the Koutecky-Levich plot shown in Figure 7b. The best fit-line of each linear regression along with its respective coefficient of determination (R^2) can as well be observed in the Figure. Very close slope values were calculated for each data set. This is because the kinetic current is observed in the absence of any mass transport limitation, which is verified by the lack of a plateau in the voltammograms [28, 49]. Table 2 shows the slope of the Koutecky-Levich-plot best-fit-line (m), the coefficient of determination (R^2) of each linear regression, the diffusion-coefficient of each synthesized surfactant calculated from Equation 2, and the percentage error (%E) of the values calculated using the standard error equation. Imidazole-based compounds show higher diffusion coefficients than those of their pyridine-base counterparts. The latter is due to the molecular weight effect and their different physicochemical properties such as viscosity, density and solubility, all related to hydrophilic-hydrophobic equilibrium within the aqueous systems [51].

The calculated diffusion coefficients can be compared with the values reported by Weinheimer [52], who published values of 4.53×10^{-6} and $6.45 \times 10^{-7} \text{ cm}^2 \text{ s}^{-1}$ for the diffusion parameters of sodium dodecyl sulfate and Triton X-100, respectively.

Table 2. Calculated diffusion coefficient of the synthesized imidazole-based- and pyridine-based-surfactants. The Koutecky-Levich analysis of the C18IMI surfactant is shown in Figure 7.

Surfactants	m	R^2	$D_0 (\text{cm}^2 \text{ s}^{-1})$	%E
C6IMI	0.0046	0.9861	2.28×10^{-6}	0.004%
C12IMI	0.0124	0.9606	7.45×10^{-7}	0.01%
C18IMI	0.0433	0.9920	1.49×10^{-7}	0.03%
C6PYR	0.0071	0.9934	1.28×10^{-6}	0.05%
C12PYR	0.0159	0.9515	5.33×10^{-7}	0.02%
C18PYR	0.0446	0.9868	1.47×10^{-7}	0.04%

As the number of carbons within the hydrocarbon chain increases, the diffusion coefficient decreases. According to the literature [53], this is attributed to the higher molecular weight and a steric effect that increases the hydrophobicity of the molecules, thus slowing-down transport towards the working electrode. On the other hand, the alkyl chain length influences the aggregation of micellar monomers favoring the formation of micelles. The latter being larger in size present a smaller transport rate within the aqueous medium.

4. CONCLUSIONS

The two-staged reaction mechanism of cation formation followed by anion exchange proved to be a straightforward route to synthesize imidazole and pyridine-based surfactants. Cyclic voltammograms showed each synthesized molecule has a characteristic electrochemical behavior, according to the attached alkyl chain length. The latter had as well a significant effect on the diffusion coefficient of each surfactant. Shorter alkyl chain lengths (C6IMI and C6PYR) were found to have a

greater ability to diffuse than those with 12- and 18-carbon chains. This could be of important value to their application, for example, in the recovery of hydrocarbon-contaminated soils.

ACKNOWLEDGMENTS

A. R. Lara-Hernández acknowledges the scholarship No. 724540 provided by CONACYT-Mexico. The authors would like to thank Projects of Scientific Development to Address National Problems (CONACYT-APN-No.3676) and Technological Development and Innovation Projects for Students (TecNM 10328.21-P) for financial support.

SUPPLEMENTARY INFORMATION

NMR spectra

C12IMI, ^1H -RMN (400 MHz, D_2O) δ (ppm): 0.98 (t, 3H), 1.28-1.31 (m, 16H), 1.37 (d, 2H), 1.90 (t, 2H), 2.37 (s, 3H), 2.76 (s, 1H), 3.37 (s, 3H), 4.62 (t, 2H), 4.74 (d, 1H), 4.78 (d, 1H), 7.47 (d, 2H), 7.94 (d, 2H). ^{13}C -RMN (100 MHz, D_2O) δ (ppm): 14.02, 21.13, 22.94, 27.37, 28.29, 28.92, 29.06, 31.65, 34.39, 46.42, 121.06, 124.29, 126.74, 128.77, 137.50, 138.31, 146.67.

C18IMI, ^1H -RMN (400 MHz, D_2O) δ (ppm): 0.99 (t, 3H), 1.14 (t, 2H), 1.29-1.37 (m, 28H), 1.90 (t, 2H), 2.38 (s, 3H), 3.41 (s, 3H), 3.74 (s, 1H), 4.62 (t, 2H), 4.76 (d, 1H), 4.80 (d, 1H), 7.47 (d, 2H), 7.93 (d, 2H). ^{13}C -RMN (100 MHz, D_2O) δ (ppm): 14.14, 21.23, 22.71, 26.23, 29.12, 29.39, 29.52, 29.69, 30.11, 31.95, 46.40, 121.74, 123.17, 125.86, 128.88, 136.86, 139.88, 142.40.

C6PYR, ^1H -RMN (400 MHz, D_2O) δ (ppm): 0.99 (t, 3H), 1.31 (d, 2H), 1.34 (d, 2H), 1.38 (d, 2H), 1.97 (t, 2H), 2.31 (s, 3H), 2.39 (s, 3H), 4.70 (t, 1H), 5.01 (d, 1H), 7.46 (d, 2H), 7.81 (m, 2H), 7.91 (d, 2H), 8.15 (t, 1H). ^{13}C -RMN (100 MHz, D_2O) δ (ppm): 13.26, 19.52, 20.52, 21.78, 25.15, 29.35, 30.47, 58.08, 124.22, 125.33, 125.54, 127.84, 129.39, 130.16, 139.63, 140.53, 146.17, 155.15.

C12PYR, ^1H -RMN (400 MHz, D_2O) δ (ppm): 0.99 (t, 3H), 1.26 (d, 2H), 1.28-1.32 (m, 14H), 1.38 (t, 2H), 2.36 (s, 3H), 2.39 (s, 3H), 4.35 (t, 1H), 5.01 (t, 1H), 7.48 (d, 2H), 7.80 (m, 2H), 7.95 (d, 2H), 8.14 (t, 1H). ^{13}C -RMN (100 MHz, D_2O) δ (ppm): 13.88, 19.22, 19.90, 20.94, 22.65, 26.19, 29.28, 29.52, 29.64, 29.86, 29.90, 30.12, 32.00, 57.82, 124.16, 125.98, 127.76, 128.78, 130.45, 139.61, 142.38, 145.02, 145.46, 154.73.

C18PYR, ^1H -RMN (400 MHz, D_2O) δ (ppm): 1.00 (t, 3H), 1.20 (t, 2H), 1.23-1.39 (m, 28H), 2.35 (s, 3H), 2.39 (s, 3H), 4.93 (d, 2H), 5.02 (d, 2H), 7.47 (d, 2H), 7.79 (d, 2H), 7.94 (d, 2H), 8.14 (t, 1H), 9.50 (m, 1H). ^{13}C -RMN (100 MHz, D_2O) δ (ppm): 14.14, 22.73, 24.47, 26.25, 28.22, 28.82, 28.95, 29.24, 29.48, 29.59, 29.66, 29.70, 29.74, 29.79, 29.87, 31.97, 32.89, 33.99, 66.06, 70.84, 76.73, 77.05, 77.36, 120.68, 123.25, 124.96, 136.23, 141.21, 146.67, 145.59, 149.13.

References

1. Y. Wang, F. Yan, Q. Jia, Q. Wang, *J. Mol. Liq.*, 253 (2018) 205.
2. Y. Shi, F. Yan, Q. Jia, Q. Wang, *Colloids Surf. A Physicochem. Eng. Asp.*, 583 (2019) 20.
3. Y. Shi, H. Qun Luo, N. Bin Li, *Spectrochim. Acta A Mol. Biomol. Spectrosc.*, 78 (2011) 1403.
4. J. K. Salem, I. M. El-Nahhal, F. S. Salama, *Chem. Phys. Lett.*, 730 (2019) p. 445.
5. S. Sadjadi, F. Koohestani, *J. Mol. Liq.*, 319 (2020) p. 114.
6. A. Abo-Hamad, M. A. AlSaadi, M. Hayyan, I. Juneidi, M. A. Hashim, *Electrochim. Acta*, 193 (2016) 321.
7. S. Sadjadi, *J. Mol. Liq.*, 323 (2020) p. 114.
8. B. V. Viada, A. V. Juárez, E. M. Pachón-Gómez, M. A. Fernández, L. M. Yudi, *Electrochim. Acta*, 263 (2017) 499.
9. Z. Wei, D. Yi, X. Hu, C. Sun, Y. Long, H. Zheng, *Colloids Surf. A Physicochem. Eng. Asp.*, 595 (2020) 124.
10. I. Ullah, K. Ahmad, A. Shah, A. Badshah, U. Ali, I. Zia-ur, S. Zeb Kan, *J Surfactants Deterg.*, 17 (2013) 13.
11. P. Lozano-Sánchez, J. M. Elliott, *Analyst*, 133 (2008) 256.
12. A. C. F. Ribeiro, C. I. A. V. Santos, D. B. Murtinho, V. M. M. Lobo, A. J. M. Valente, *J. Chem. Thermodyn.*, 50 (2012) 89.
13. Z. Xun, C. Cai, T. Lu, *Electroanalysis*, 16 (2004) 674.
14. L. Fernández, H. Carrero, *Electrochim. Acta*, 50, (2005) 1233.
15. L. Stroea, T. Buruiana, E. Buruiana, *Mater. Chem. Phys.*, 223 (2019) 311.
16. L. Andreani, J. D. Rocha, *Brazilian J. Chem. Eng.*, 29 (2012) 1.
17. S. V. Malhotra, T. Welton, *Ionic Liquids in organic synthesis*, (2007), ACS: American Chemical Society, Washington D. C., United States of America.
18. E. Thomas, D. Thomas, S. Bhuvaneshwari, K.P. Vijayalakshmi, B. K. George, *J. Mol. Liq.*, 249 (2017) 404.
19. Y. X. Sun, Y. Y. Wang, B. B. Shen, B. X. Zhang, X. M. Hu, *Chem. Sci.*, 5 (2018) 181.
20. M. Kumar-Banjare, R. Kurrey, S. Sinha, M. Satnami, K. Ghosh, *J. Mol. Liq.*, 241 (2017) 622.
21. D. Zhao, Z. Fei, R. Scopelliti, P. J. Dayson, *Inorg. Chem.*, 43 (2004) p. 2197.
22. R. K. Mahajan, N. Kaur, M. S. Backshi, *Colloids Surf. A Physicochem. Eng. Asp.*, 255 (2005) 33.
23. C. Racaud, K. Groenen-Serrano. A. Savall, *J. Appl. Electrochem.*, 40 (2010) 1845.
24. R. Sanjay, S. Sengupta, S. Partha, *Chem. Phys. Lett.*, 694 (2018) 7.
25. I. Berlot, P. Labbé, P. Letellier. J. Moutet, M. Turmine, *J. Electroanal. Chem.*, 43 (1997) 57.
26. K. Santana-Barros, E. M. Ortega, V. Pérez-Herranz, D. C. Romano Espinosa, *J. Electroanal. Chem.*, 856 (2020) 114.
27. S. Treimer, A. Tang, D. C. Johnson, *Electroanalysis*, 14 (2002) 165.
28. N. Aouina, H. Cachet, C. Debiemme-chouvy, T. T. Mai-Tran, *Electrochim. Acta*, 55 (2010) 7341.
29. J. M. Lazaro-Martínez, M. F. Leal Denis, V. Campo Dall'Orto, G. Y. Buldain, *Eur. Polym. J.* 44 (2008) 392.
30. V. S. Kumar, Y. S. Mary, K. Pradhan, D. Brahman, Y. S. Mary, R. Thomas, M. S. Roxy, C. Van del Alsenoy, *J. Mol. Struct.*, 1199 (2020) 127.
31. S. M. Caroline Diana, M. R. Rekha, *Int. J. Biol. Macromol.*, 105 (2017) 947.
32. T. Huang, W. Zhao, X. Zhang, X. Nie, J. Chen, W. Xiong, *J. Mol. Liq.*, 320 (2020) 114.
33. Y. Chesalov, T. Andrushkevich, V. Sobolev, G. Chernobay, *J. Mol. Catal. A Chem.*, 380 (2013) 118.
34. M. Liu, S. Gou, Q. Wu, X. Yang, Y. He, L. Zhou, L. Tang, L. Liu, M. Duan, *J. Mol. Liq.*, 296 (2019) 111.
35. R. Golla, P. Raghavendra, P. A. Suchethan, S. Foro, G. Nagaraju, *J. Mol. Struct.*, 1201 (2019) 127.
36. T. Asakawa, H. Sunagawa, S. Miyagishi, *Langmuir* 14 (1998) 7091.
37. J. Luczak, J. Hupka, J. Thoming, C. Jungnickel, *Colloids Surf. A Physicochem. Eng. Asp.*, 329 (2008)

125.

38. Z. X. Chen, S. P. Deng, X. K. Li, *J. Colloid Interface Sci.*, 318 (2008) 389.
39. M. A. Rather, G. M. Rather, S. A. Pandit, S. A. Bhat, M. A. Bhat, *Talanta*, 131 (2015) 55.
40. H. Xiao, W. Wang, S. Pi, Y. Cheng, Q. Xie, *Anal. Chim. Acta*, 1137 (2020) 20.
41. M. T. García, I. Ribosa, L. Pérez, A. Manresa, F. Comelles, *Langmuir*, 29 (2013) 2536.
42. S. Javadian, F. Nasiri, A. Heydari, A. Yousefi, A. A. Shadir, *J. Phys. Chem. B*, 118 (2014) 4140.
43. M. Blesic, M. H. Marques, N. V. Plechvoka, K. R. Seddon, L. P. N. Rebelo, A. Lopes, *Green Chem.*, 9 (2007) 481.
44. H. Xiao, W. Wang, S. Pi, Y. Cheng, Q. Xie, *Sens. Actuators B Chem.*, 317 (2020) 128.
45. B. Dong, X. Zhao, L. Zheng, J. Zhang, N. Li, T. Inoue, *Colloids Surf. A Physicochem. Eng. Asp.*, 317 (2008) 666.
46. K. Kinoshita, E. Parra, D. Needham, *J. Colloid Interface Sci.*, 504 (2017) 765.
47. P. D. Galgano, O. A. El-Soud, *J. Colloid Interface Sci.* 361 (2011) 186.
48. Y. Sun, X. Xu, M. Qin, N. Pang, G. Wang, L. Zhuang, *Colloid Polym. Sci.*, 297 (2019) 571.
49. A. J. Bard; L. A. Faulkner, *Electrochemical Methods: Fundamentals and Applications* (2000), 2nd ed. Wiley-Interscience, New York, United States of America.
50. J. Kim, A. J. Bard, *Anal. Chem.*, 88 (2016) 1742.
51. I. D. Charlton, A. P. Doherty, *Anal. Chem.*, 72 (2000) 687.
52. R. M. Weinheimer, D. Fennell-Evans, E. L. Cussler, *J. Colloid Interface Sci.*, 80 (1980) 357.
53. O. Cusola, C. Valls, T. Vidal, T. Tzanov, M. B. Roncero, *ACS Appl. Mater. Interfaces*, 138 (2015) 34.

© 2021 The Authors. Published by ESG (www.electrochemsci.org). This article is an open access article distributed under the terms and conditions of the Creative Commons Attribution license (<http://creativecommons.org/licenses/by/4.0/>).